




# Convergent evolution among non-carnivorous, desert-dwelling theropods as revealed by the dentary of the noosaurid *Berthasaura leopoldinae* (Cretaceous of Brazil)

by FELIPE FERREIRA PIEROSS<sup>1</sup> , RAFAEL DELCOURT<sup>1,\*</sup> , DANIEL DE MELO CASALI<sup>1</sup> , JOÃO ALBERTO LEME<sup>1</sup>, NEURIDES DE OLIVEIRA MARTINS<sup>2</sup>, PAULO MANZIG<sup>2</sup> and MAX CARDOSO LANGER<sup>1</sup>

<sup>1</sup>Laboratório de Paleontologia, Faculdade de Filosofia, Ciências e Letras de Ribeirão Preto, Departamento de Biologia, Universidade de São Paulo, Av. Bandeirantes, 3900, 14040-901 Ribeirão Preto, SP, Brazil; [rafael.delcourt@gmail.com](mailto:rafael.delcourt@gmail.com)

<sup>2</sup>Museu de Paleontologia de Cruzeiro do Oeste 'Alexandre Gustavo Dobruski', R. João Ormino de Rezende, 686, 87400-000 Cruzeiro do Oeste, PR, Brazil

\*Corresponding author

Typescript received 3 November 2024; accepted in revised form 7 May 2025

**Abstract:** The Cretaceous witnessed the establishment of many desertic landscapes across the globe, including the Early Cretaceous Caiuá palaeodesert, in south-central Brazil, and those of several Late Cretaceous deposits of the Gobi Desert. Although separated in time and space, their faunas share the presence of medium-sized, edentulous theropods (e.g. oviraptorids and *Berthasaura leopoldinae*) which depart from the typically carnivorous diet of the group. Here, we report a new dentary of the latter taxon, which bears alveolar vestiges, suggesting that its teeth were lost during ontogeny, as previously reported for another noosaurid, *Limusaurus inextricabilis*,

from the Late Jurassic of China. In addition, we used geometric morphometrics to quantitatively analyse the shape of theropod jaw bones, revealing a significant morphological convergence signal for the dentary of *Be. leopoldinae* and oviraptorids, which are dorsoventrally deep, and bear a large mandibular fenestra. This probably resulted from adaptations to feed on the tough parts of xerophytic plants, which are important food sources in desertic environments.

**Key words:** Theropoda, Noosauridae, convergent evolution, skull, geometric morphometrics, diet.

THEROPOD dinosaurs represent one of the most successful lineages of predatory vertebrates (Hendrickx *et al.* 2015; Cau 2024). Yet, this ancestral behaviour changed several times along their evolutionary history (Ma *et al.* 2022), with numerous birds (Miller & Pittman 2021), as well as non-avian groups such as alvarezsaurids (Longrich & Currie 2009), ornithomimosaurs (Barrett 2005), noosaurids (Xu *et al.* 2009), therizinosauroids (Lautenschlager 2017), oviraptorosaurs (Meade & Ma 2022), and even some troodontids (Cullen & Couzens 2024), having a diet not exclusively based on meat. Among these, oviraptorids bear peculiarly deep, pneumatized skulls, with toothless jaws capable of very strong bites (Meade & Ma 2022). Recent studies agree that these theropods were at least partially herbivorous (Smith 1992; Ji *et al.* 1998; Xu *et al.* 2002; Barrett 2005; Longrich *et al.* 2010), most probably feeding on tough plant items such as stems, nuts or seeds (Meade & Ma 2022). This fits the apparent preference of the group for arid to semi-arid environments (Hasegawa *et al.* 2009; Tsuihiji

*et al.* 2016), in which xerophytic vegetation is presumably prevalent (Longrich *et al.* 2010).

In recent years, several studies have revealed a unique desert-dwelling fauna coming from the Lower Cretaceous Caiuá Group, in south-central Brazil (Fernandes *et al.* 2007; Ernesto *et al.* 2024). This is so far represented by a single outcrop, the 'Cruzeiro do Oeste Palaeontological Site', located in the eponymous town, which has yielded pterosaurs (Manzig *et al.* 2014; Kellner *et al.* 2019; Pêgas 2025), dinosaurs (Langer *et al.* 2019; de Souza *et al.* 2021), and one lizard (Simões *et al.* 2015). Here, we report an isolated dentary (MPCO. V 0121) from that site, ascribed to the noosaurid dinosaur *Berthasaura leopoldinae* (de Souza *et al.* 2021), which shares general traits with those of oviraptorids. This provided the opportunity to investigate the morphology of the theropod jaw apparatus on a quantitative basis, aiming to identify possible convergence events between edentulous/desert-dwelling members of the group. Other studies applying geometric morphometrics to analyse the

theropod skull have been carried out before (e.g. Marugá n-Lobón & Buscalioni 2004; Brusatte *et al.* 2012; Foth & Rauhut 2013; Ma *et al.* 2022), but they are typically broader in scope, not focusing on specific bones or an evolutionary hypothesis, as attempted here.

## MATERIAL & METHOD

### New fossil material

Left dentary (MPCO. V 0121; Museu de Paleontologia de Cruzeiro do Oeste, Brazil) missing the surangular ramus and the tip of the ventral ramus (Fig. 1). The fossil comes from the 'Cruzeiro do Oeste Paleontological Site' (Langer *et al.* 2019), informally called 'Cemitério dos Pterossauros Quarry' (Kellner *et al.* 2019), which is the same site that yielded the holotype of *Be. leopoldinae* (MN 7821-V; Museu Nacional Universidade Federal do Rio de Janeiro, Brazil; de Souza *et al.* 2021). That outcrop exposes sedimentary rocks formed by the influence of water bodies, most likely in interdune settings, within the primarily aeolian deposits of the Caiuá Group, which represents a desert palaeoenvironment (Fernandes *et al.* 2007) and is Early Cretaceous in age (Ernesto *et al.* 2024).

### 3D reconstruction

The material was scanned at 'Centro para Documentação da Biodiversidade', Universidade de São Paulo at Ribeirão Preto, using a micro-CT GE Phoenix|tome|x

S240 scanner, with 1000 projections, exposure time of 0.3 s, voltage of 130 Kv, and a current of 150  $\mu$ A, with a voxel size of 25.8  $\mu$ m. Segmentation was carried out using Amira v5.3.2 (ThermoFischer Scientific). For each slide generated by the  $\mu$ CT-scan, areas with intensity values (Amira's measurement unit of density in CT-scanned volumes) ranging from 19 to 23 were selected and traced. This corresponds to internal parts of the material with density low enough to probably represent cavities within the bone, which were grouped into a single object and segmented into a 3D model. This was combined with the previously generated isosurface, producing a translucent model of the dentary with its internal cavities highlighted in yellow (Fig. 2). The raw  $\mu$ CT scan data (.dcm) is available in MorphoSource (Pierossi *et al.* 2025a).

### Geometric morphometric data acquisition

The maxilla and dentary images used in this study were obtained from published articles, as well as from photographs taken first hand by the authors (Appendix S1). Such images mainly correspond to the original fossils, but reconstructions were used for taxa that lack fully preserved bones. In the case of *Be. leopoldinae*, we employed the right dentary of its holotype, figured by de Souza *et al.* (2021, fig. 2o), which is the most completely known for the taxon. The morphological variation of the specimens was assessed with two-dimensional geometric morphometrics. This method allows us to mathematically quantify the morphological disparity between biological

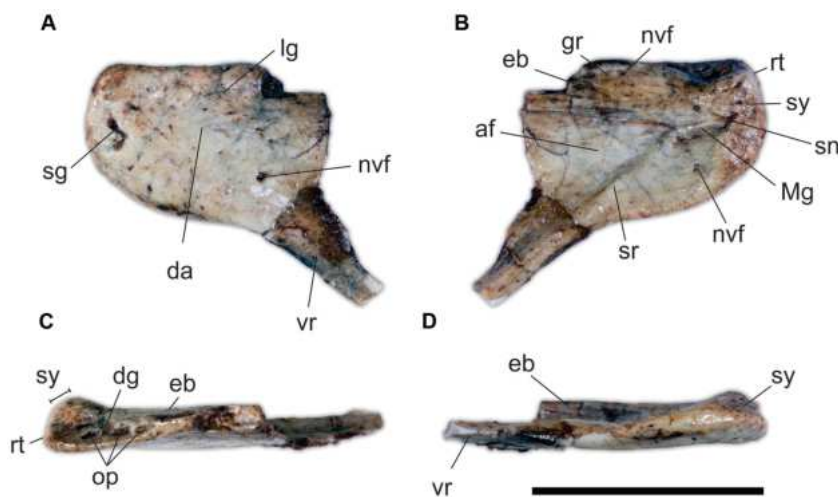


**FIG. 1.** Left dentary (MPCO. V 0121) of *Berthasaura leopoldinae* in: A, lateral; B, medial; C, occlusal; D, ventral view. *Abbreviations:* af, adductor fossa; da, depressed area; dg, dorsal groove; eb, elongated bulge; gr, groove; lg, lateral groove; Mg, Meckelian groove; nvf, main neurovascular foramina; op, occlusal pits; rt, rostral tip; sg, sigmoid groove; sn, symphyseal notch; sr, splenial ridge; sy, symphysis; vr, ventral ramus. Scale bar represents 2 cm.

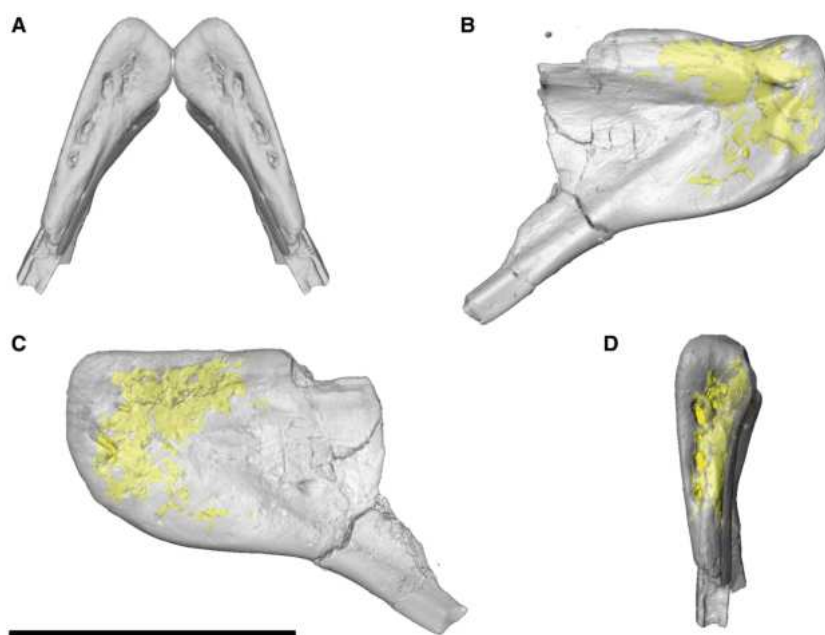


**FIG. 2.** Digital reconstruction from  $\mu$ CT-scan images of MPCO. V 0121 (left dentary of *Berthasaura leopoldinae*). A, isosurface of the bone in dorsal view, mirrored to the right side to show the angle formed by the pair. B–D, translucent model in medial (B), lateral (C), and dorsal (D) view, with internal cavities highlighted in yellow. Scale bar represents 2 cm. Digital reconstruction from  $\mu$ CT-scan images of MPCO. V 0121 (left dentary of *Berthasaura leopoldinae*). A, isosurface of the bone in dorsal view, mirrored to the right side to show the angle formed by the pair. B–D, translucent model in medial (B), lateral (C), and dorsal (D) view, with internal cavities highlighted in yellow. Scale bar represents 2 cm.

elements and is also useful to remove size related variation from the shape of the specimens (O'Higgins 2000).

The studied maxillae and dentaries were scored in two separate datasets. Dataset 1 includes 65 maxilla samples, each representing a single species, scored for 12 homologous landmarks (Fig. 3). These were chosen for their anatomic importance (e.g. most rostral point of the maxillary fossa) or value as a definer of bone shape (e.g. main inflection point of the ascending ramus). Dataset 2 is composed of 52 dentary samples scored for 11 landmarks (Fig. 3). As most species were included in both datasets, the total number of sampled species is 69 (see Appendix S1). In order to include edentulous forms, such as oviraptorids, some ornithomimosaurs, and *Be. leopoldinae*, no landmarks used in this study were related to the teeth. The landmarks were manually plotted on the samples using the TpsDig2 software, v2.32 (Rohlf 2010), and their descriptions are provided in Appendix S2.

#### Dietary & taxonomic group definitions

The studied species were separated into dietary and taxonomic groups. For diet, they were divided into 'carnivores' and 'non-carnivores', following the general

consensus of the scientific literature, even though some employed taxa have dubious feeding habits (Zanno & Makovicky 2011; Freimuth *et al.* 2021; Cullen & Couzens 2024). 'Carnivores' includes all taxa that fed mainly on other vertebrates, whereas 'non-carnivores' encompass the remaining taxa. Diets were defined for almost all species in the sample based on Zanno & Makovicky (2011), either using information for single taxa (e.g. *Byronosaurus jaffei*) or extrapolating clade diets to individual species (e.g. Tyrannosauroidea). The only 'non-carnivore' defined from another source was *Be. leopoldinae* (de Souza *et al.* 2021), with all other species not discussed by Zanno & Makovicky (2011) considered as 'carnivores' given the ancestral diet for theropods (Ma *et al.* 2022) and the lack of contrary evidence. In order to maximize the number of taxonomic groups, whilst avoiding overly small sample sizes per group (as needed for the statistical analysis), both non-monophyletic (identified with quotation marks) and monophyletic groups were defined: 'non-Averostra Theropoda' (You *et al.* 2014; Hendrickx *et al.* 2015), Ceratosauria (Hendrickx *et al.* 2015; Zaher *et al.* 2020, de Souza *et al.* 2021), 'non-Coelurosauria Tetanurae' (Allain 2002; Hendrickx *et al.* 2015; Canale *et al.* 2022), Tyrannosauroidea + Megaraptora (Brusatte & Carr 2016; Aranciaga Rolando *et al.* 2022), Paraves (Jasinski *et al.* 2020),

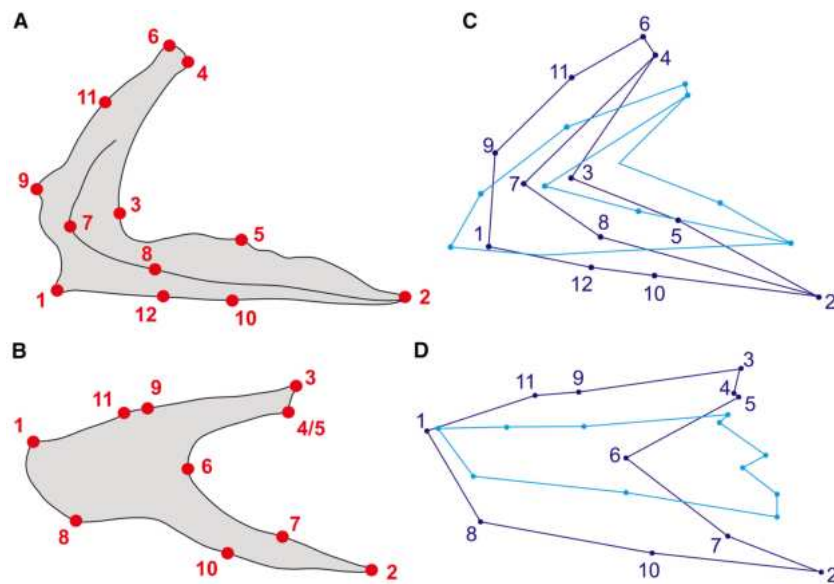


**FIG. 3.** A–B, landmarks used in the current study figured over the maxilla (A) and dentary (B) of the *Berthasaura leopoldinae* holotype, reconstructed based on de Souza *et al.* (2021). C–D, images of the respective bones made with the software R (R Core Team 2024); dark blue lines and points represent the shape of the *Be. leopoldinae* bones; light blue lines and points indicate the mean shape of all theropods in the sample.

‘non-Pennaraptora Maniraptoromorpha’ (Hendrickx *et al.* 2015; Xing *et al.* 2020; Cuesta *et al.* 2022), and Oviraptorosauria (Lü *et al.* 2015).

‘Non-Averostra Theropoda’ clusters small to medium sized theropods that lived during the Triassic and Early Jurassic (Sereno & Novas 1994; Nesbitt *et al.* 2009; Sues *et al.* 2011; Marsh & Rowe 2020). ‘Non-Coelurosauria Tetanurae’ comprises early diverging, medium to large hyper-carnivorous tetanurans, including Megalosauroida (Carrano *et al.* 2012) and Allosauroida (Brusatte & Sereno 2008). ‘Non-Pennaraptora Maniraptoromorpha’ includes small-bodied carnivorous theropods such as Compsognathidae (Sales *et al.* 2014), the non-carnivores Ornithomimosauria and Therizinosauria (Barrett 2005; Lautenschlager 2017), as well as other taxa such as *Scipionyx samniticus* and *Haplocheirus sollers*.

#### Theropoda supertree

As a basis to estimate evolutionary rates and ancestral diets, an informal phylogenetic tree was built, containing all taxa used in the study (Fig. 4). The tree was assembled using the software Mesquite v3.81 (Maddison & Maddison 2023), with the species positions based on the most up to date information available for each of them (Allain 2002; You *et al.* 2014; Hendrickx *et al.* 2015; Lü *et al.* 2015; Brusatte & Carr 2016; Jasinski *et al.* 2020; Xing *et al.* 2020; Zaher *et al.* 2020; de Souza *et al.* 2021;

Aranciaga Rolando *et al.* 2022; Canale *et al.* 2022; Cuesta *et al.* 2022); see Appendix S3 for further details.

#### Time-calibration of the supertree

First (FAD) and last (LAD) appearance data for each species included in the supertree were obtained from the Paleobiology Database (PBDB; <https://paleobiodb.org/#/>) and used to time-calibrate the tree. We employed a clock-less and ‘empty matrix’ Bayesian tip-dating approach, applying the fossilized birth–death process (FBD) in MrBayes v3.2.7a (Ronquist *et al.* 2012; Zhang *et al.* 2016). In that process, all taxa were scored as ‘?’ for a single character and the supertree topology was included via a series of backbone constraints with the aid of the function createMrBayesTipDatingNexus in the R (v4.3.3; R Core Team 2024) package paleotree v3.4.7 (Bapst 2012). During the time-calibration analysis, polytomies were randomly resolved. The age for each taxon was sampled from a uniform distribution defined by the respective FAD–LAD interval. For the root age, we considered a uniform distribution ranging from the FAD of the operational outgroup (i.e. *Herrerasaurus ischigualastensis*) to 10 million years before (uniform (228, 238)). Prior distributions for the FBD parameters were set to: speciationpr = uniform (0,10), extinctionpr and fossilizationpr = beta (1,1). We disallowed sampling taxa as ancestors (samplestrat = fossiltip), because downstream



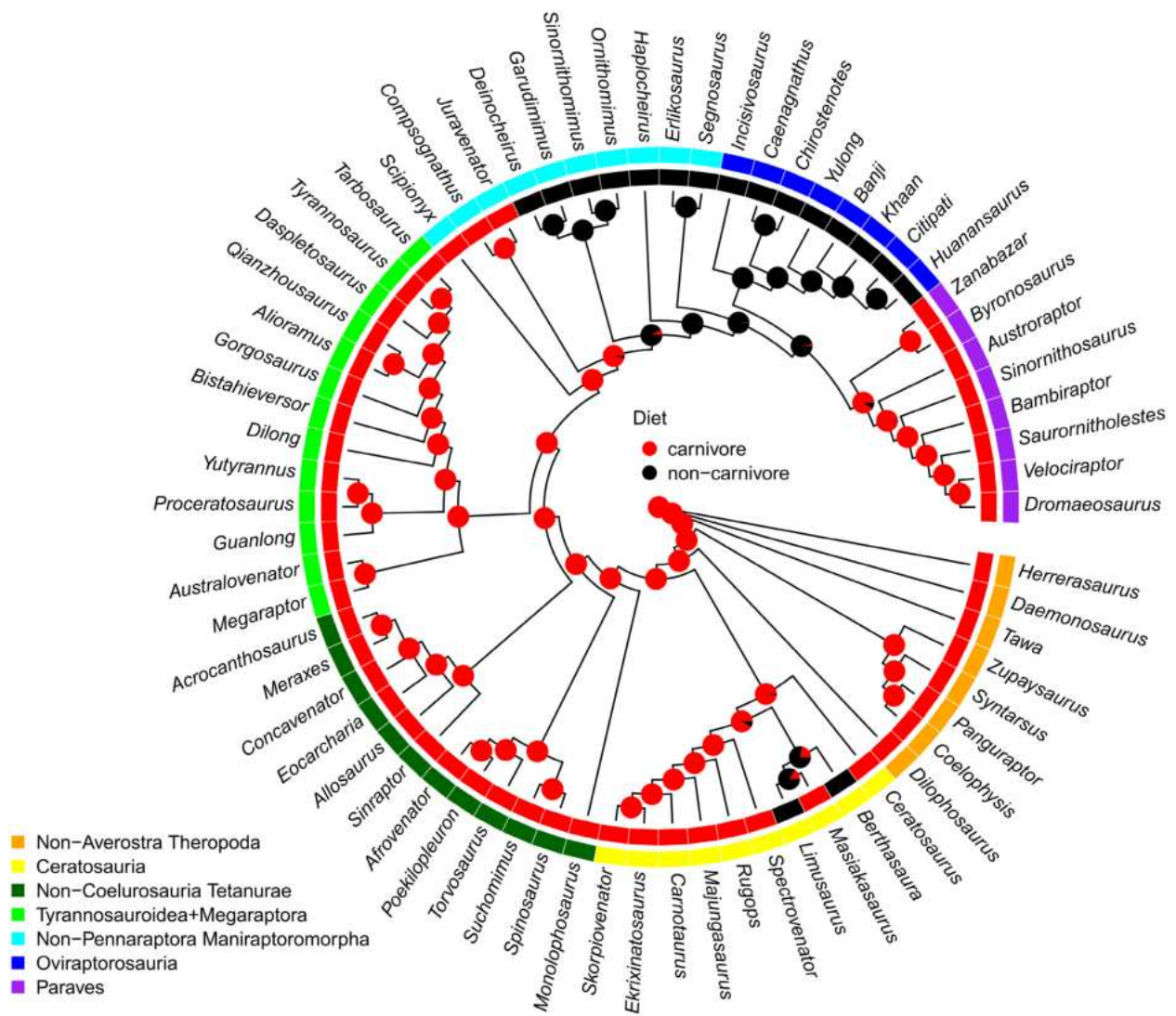


**FIG. 4.** The adopted phylogeny including only the sampled species of Theropoda, with pies indicating the probabilities of ancestral diets at the nodes. The inner external circle indicates the dietary category for each taxon and the outermost circle the taxonomic group, as applied in our analyses. The adopted phylogeny including only the sampled species of Theropoda, with pies indicating the probabilities of ancestral diets at the nodes. The inner external circle indicates the dietary category for each taxon and the outermost circle the taxonomic group, as applied in our analyses.

macroevolutionary analyses requires trees with positive branch lengths. To account for the fact that all sampled taxa are extinct, we set a very small value for the proportion of extant taxa sampled (sampleprob = 0.001), as a positive value is required in the implementation of FBD in MrBayes. Markov chain Monte Carlo (MCMC) sampling was performed with two independent runs of 100 million generations and with four chains (one cold and three heated) each, sampling at every 5000th generation. The initial 10% of the samples were discarded as a burn-in phase, and convergence was accessed in MrBayes, monitoring the potential scale reduction factor (PRSF)  $\approx 1.0$  and estimated sample sizes (ESS) of at least

100. ESS values for FBD parameters and tree height were  $>1000$ , whereas for tree length, given the absence of a clock and character data, an ESS of 100 was considered sufficient. The Nexus input file and the resulting time-calibrated trees are available in the Dryad Digital Repository (Pierossi *et al.* 2025b).

#### Macroevolutionary analyses

All macroevolutionary analyses were conducted in the R programming environment. Unless stated otherwise, analyses were carried out with functions of the package

geomorph v4.0.7 (Adams *et al.* 2024), which rely extensively on the package RRPP v2.0.0 (Collyer & Adams 2024). For all geomorph analyses, significance was assessed by 1000 permutations ( $\alpha = 0.05$ ). Summary and test statistics across the 100 randomly sampled time-calibrated trees were summarized using the median and 95% CI values. Other employed packages were: phytools v2.3.0 (Revell 2024) and ggplot2 v2 3.5.1 (Wickham 2016), to make plots; rstatix v0.7.2 (Kassambara 2023) to calculate summary statistics; and openxlsx v4.2.5.2 (Schauberger & Walker 2023) to export tables; we also used a customized version of the ggphylo-morpho function (Barr 2017). The R script and associated input files necessary to fully reproduce all analyses and plots, including the landmarks files, the tree files, and information about the age range and group assignments for each taxon, are available in the Dryad Digital Repository (Pierossi *et al.* 2025b).

#### *Ancestral diet estimations*

Using a maximum likelihood approach, we inferred ancestral diets on our supertree, employing both equal (ER) and unequal (ARD) rate variations of the MK model of discrete trait evolution (Pagel 1994; Lewis 2001; Paradis *et al.* 2004). For each model, we calculated the Akaike information criterion (AIC) and summarized the results in the proportion of the respective support (i.e. AIC weights) using a model averaging procedure in package phytools (Revell 2024).

#### *Exploratory morphometric analyses*

To remove the effects of scale, position and orientation, the landmark data was superimposed with a generalized Procrustes analysis (GPA). Procrustes coordinates were then submitted to a principal component analysis (PCA), and a bidimensional phylomorphospace was used to visually inspect the distribution of taxa in the first two PCs; see Table S2 for all PCA results.

#### *Phylogenetic signal & allometry*

The phylogenetic signal in the Procrustes coordinates was quantified using the multivariate extension of the widely used K-statistic, K-multi (Blomberg *et al.* 2003; Adams 2014a). We employed phylogenetic multivariate regressions to assess if the specimen size significantly influences its shape; respectively represented by the natural logarithm of the centroid size (obtained in GPA procedures) and Procrustes coordinates (Adams 2014b).

These regressions account for the phylogenetic effects and assume a Brownian motion (BM) model of continuous trait evolution (Felsenstein 1985).

#### *Phylogenetic regressions*

To test for the correlation of both taxonomy and diet with shape variation in the maxilla and dentary, we employed a series of phylogenetic generalized least squares (PGLS) regressions (Adams 2014b). These regressions always consider phylogenetic signal, allowing its effects to be statistically controlled (Symonds & Blomberg 2014). Using a sequential sum of squares approach, we created models in which the relationship between the shape and size of the bone were tested first, followed by testing of the relationship between that shape and the taxonomic and dietary groups. This statistically excludes the influence of size, so that only the shape effects related with those two groups were considered. As for the taxonomic groups, each was individually compared to the remainder of the taxa. Finally, we also investigated for interaction effects of size with these variables (i.e. taxonomic and dietary groups).

#### *Morphological disparity & evolutionary rates*

Procrustes variance (Zelditch *et al.* 2012) was employed to quantify the maxilla and dentary shape disparity for the dietary and taxonomic groups mentioned above. Disparity values were first calculated per group (taxonomic and dietary) and for both datasets. These values were then compared with their respective parallels (e.g. carnivores vs non-carnivores), aiming to find the statistically significant variations. For these analyses, objects fitted in allometry analyses were used as inputs, as to account for both phylogeny and size, while calculating shape disparity. Likewise, morphological evolutionary rates for these groups were calculated using a BM model, also accounting for size and phylogeny (Adams 2014c), followed by a comparison between these values. Rate values were plotted in a  $\log_{10}$  scale for easier visualization.

#### *Morphological convergence*

The relative positions of the species in the previously generated phylomorphospaces (Fig. 5) were visually inspected in search of morphological convergence hypotheses. Species were chosen for comparison if they have considerable spatial proximity in the phylomorphospace, but no close phylogenetic affinity. For the dentary, the negative end of PC1 is occupied by *Be. leopoldinae*, and the oviraptorids

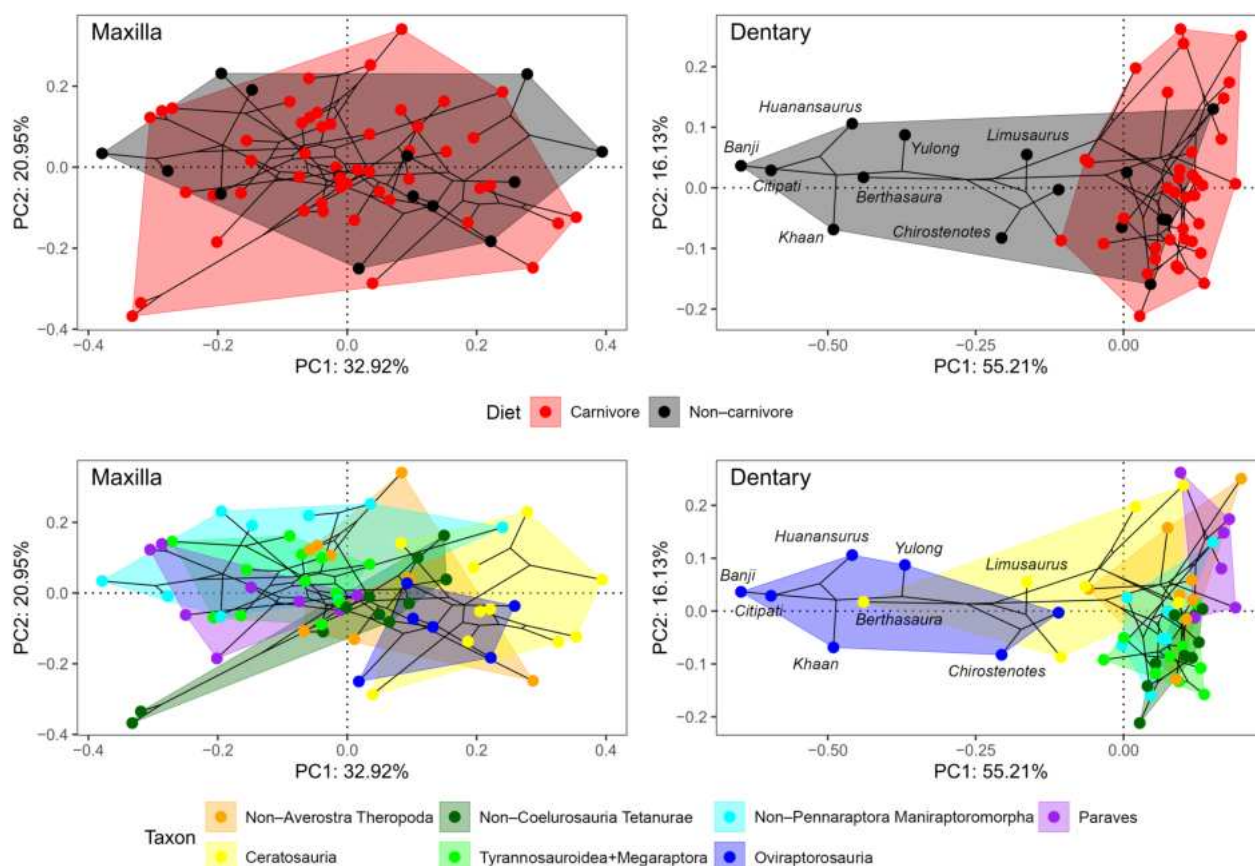


**FIG. 5.** Phylomorphospaces depicting the first two principal components (PCs) for the maxilla and the dentary, coloured by dietary and taxonomic groups. Selected taxa are indicated in the dentary plot. (See Figs S3–S6 for all taxon names.)

*Citipati osmolkae*, *Huanansaurus ganzhouensis*, *Khaan mckennai*, *Banji long* and *Yulong mini*, which were considered to be converging towards this region. For the maxilla, the troodontids *By. jaffei* and *Zanabazar junior* and the tyrannosaurid *Qianzhousaurus sinensis* converge towards the same region of the phylomorphospace. Accordingly, two convergence tests were carried out: one comparing the dentary of *Be. leopoldinae* with those of the above oviraptorids and another comparing the maxilla of *Q. sinensis* with those of *By. jaffei* and *Z. junior*. Two sets of tests were carried out: one considering all the main components that together explain at least 95% of the variation in the dataset (ten for the maxilla and seven for the dentary) and another considering only PC1 and PC2. These hypotheses were submitted to statistical tests using Ct1–Ct4 metrics (Grossnickle *et al.* 2024), which are modified versions of the original C1–C4 metrics of Stayton (2015). These quantify how much of the original distance between pairs of taxa has been closed by subsequent convergent evolution (Stayton 2015; Grossnickle *et al.* 2024). The modified metrics, unlike the original ones, limit the calculations of the maximum distance between two lineages to synchronous time-slices, which

coincide with nodes in the phylogeny. They have been shown to be much less prone to falsely support convergence than the original metrics in scenarios of divergence, parallel evolution, or only incomplete convergence (Grossnickle *et al.* 2024). Significance was assessed with 200 simulations for each tree ( $\alpha = 0.05$ ).

## RESULTS

### Anatomical description

Although slightly smaller (c. 5% shallower dorsoventrally), the left dentary MPCO. V 0121 (Figs 1, 2) is very similar to those of the holotype of *Be. Leopoldinae* (de Souza *et al.* 2021), including a main body and an elongate ventral ramus. The former is deep dorsoventrally and short rostrocaudally, with rounded rostral margin and rostroventral corner and straight dorsal and ventral margins, angled c. 10° to one another. The ventral ramus extends caudoventrally at an angle of about 45° relative to the occlusal margin of the bone, tapering distally and missing its tip. The dorsal margin of that ramus, along with the caudal margin of the body are



complete, forming the rostroventral and rostral margins of a large mandibular fenestra. Dorsal to that, however, the bone is broken, lacking the entire surangular ramus. At large, the dentary is lateromedially flattened, but more robust along its dorsal and rostral margins, which expand medially forming the occlusal and symphyseal areas, respectively. The bone is laminar ventrocaudal to that, given the excavation of its medial surface. This area is pierced by a neurovascular foramen caudal to the ventral portion of the symphysis. Yet, unlike those of other theropods (Sampson & Witmer 2007), this foramen is ventrorostrally oriented in MPCO. V 0121.

The lateral surface of the dentary is mostly flat, with a subtle rostrocaudally oriented groove ('lg' in Fig. 1), extending below the caudal half of its dorsal margin, and a slightly depressed central area ('da' in Fig. 1), ventral to that. Several small foramina are randomly distributed across the lateral surface of the bone, with a larger one placed near the base of the ventral ramus. Unlike the holotype of *Be. leopoldinae*, MPCO. V 0121 lacks a curved row of large foramina near the rostral edge of the bone, but bears a deep sigmoid groove ('sg' in Fig. 1), in that area, which seems to represent the confluence of at least two large foramina, caudal to which four small foramina are aligned on a curve following the ventral margin of the bone. As pointed out by de Souza *et al.* (2021), the abundance of foramina in the rostral portion of the dentary suggests the presence of a rhamphotheca.

As already mentioned, the medial surface of MPCO. V 0121 is marked by medially expanded rostral and dorsal areas. The former corresponds to the symphysis, which, apart from occupying the rostral margin, also expands caudally from its dorsal portion, forming a rough '7' shape. Its horizontal segment extends more caudally than that of the *Be. leopoldinae* holotype (de Souza *et al.* 2021, fig. 2o) and is somewhat continuous to the rostrocaudally elongated bulge ('eb' in Fig. 1), that extends along the dorsal margin of the bone, medially bounding the groove on its occlusal surface (see below). A very subtle groove ('gr' in Fig. 1), extends along the medial surface of the bulge, which is also pierced by a foramen. Rostral to the dorsal portion of the symphysis, there is a small, medially free area that extends rostrally when the dentaries are in articulation ('rt' in Fig. 1). Indeed, the angle formed between the articulation plane of the symphysis and the long axis of the dentary is *c.* 25° in dorsal view, indicating that the pair of bones were angled about 50° when articulated to one another (Fig. 4). The junction of the caudal and ventral segments of the symphysis is notched at its caudal margin ('sn' in Fig. 1), giving rise to a subtle Meckelian groove (Carrano *et al.* 2002), that extends caudally along the depressed portion of the dentary to reach a subtriangular and further depressed portion of that surface. This corresponds to the adductor fossa (Sampson & Witmer 2007),

which is bound dorsally by the 'elongated bulge' and ventrally by the splenial ridge (Sampson & Witmer 2007). The latter enters the medial surface of the dentary body as a rostradorsal continuation of its ventral ramus. The splenial articulation occupies the depressed areas both dorsal and ventral to the adductor fossa. The holotype of *Be. leopoldinae* also bears a subtriangular adductor fossa and a marked splenial ridge (de Souza *et al.* 2021, fig. 2o). Yet, the structure marked as the Meckelian canal in the original description is not in its expected position, as seen in MPCO. V 0121, and may instead correspond to alveolar vestiges modified into a canal, as seen in *Limusaurus inextricabilis* (Wang *et al.* 2017).

The dorsal outline of the dentary is caudally tapering, with the occlusal surface bearing a longitudinal groove ('dg' in Fig. 1), that also tapers caudally. The rostral portion of the groove is medially expanded, and also more deeply excavated, reaching the medial surface of the dentary right between the symphysis and the 'elongated bulge'. Visual inspection suggests that the lateral edge of the occlusal groove is pierced by three rostrocaudally aligned elongated pits. The rostral two of which are subequal (slightly below 2 mm long rostrocaudally), whereas the caudalmost is slightly smaller (slightly over 1 mm long). The rostralmost pit is positioned on the lateromedially broader portion of the groove and the caudal two along its tapering portion. The tracing of these pits based on the  $\mu$ CT-scan data reveal that they penetrate the dentary in the form of irregular subvertical canals (Fig. 2). Yet, there is no sign of any denser material (i.e. tooth remains) inside these canals. Moreover, the  $\mu$ CT data reveals three other pits piercing the occlusal surface of the dentary, a large one in the depressed area rostromedial to the first pit and two smaller ones, one rostromedial to that just mentioned and another rostral to the penultimate pit, all of which also lead to subvertical canals. The canals are all ventrally connected to a rostrocaudally elongated maze of cavities and/or less dense material inside the bone (Fig. 2), which in places forms subvertical walls, somewhat resembling the volumes depicted as palish areas in the CT reconstructions of the *L. inextricabilis* dentary (Wang *et al.* 2017). In MPCO. V 0121, this maze is connected to some foramina both on the medial and, especially, lateral surfaces of the bone, so that it is at least partially neurovascular in origin.

De Souza *et al.* (2021) identified 'cavities within the trabecular bone connected with the outer bone surface by foramina' in the holotypic dentary of *Be. Leopoldinae*. Yet, no discrete pits are seen in the occlusal view of the bone (de Souza *et al.* 2021, fig. 3b). That individual was considered to be a young sub-adult, comparable to *L. inextricabilis* ontogenetic stages III–IV (de Souza *et al.* 2021), an inference that, given the comparable specimen sizes, can be broadly extended to MPCO. V 0121.



Ontogenetic stage IV of *L. inextricabilis* lacks teeth or individual alveolar vestiges, bearing instead a rostrocaudally extending canal inside the dentary (Wang *et al.* 2017). Given their shape and distribution, we interpret the occlusal pits of MPCO. V 0121 and their ventral extensions as alveolar vestiges. These are absent in MN 7821-V and stage IV of *L. inextricabilis*, so that (matching its marginal smaller size) MPCO. V 0121 probably represents an earlier ontogenetic stage of *Be. leopoldinae*, in which teeth have already been reabsorbed as in MN 7821-V, but individual alveolar vestiges still remain. Such vestiges are connected to the vascular maze in the dentary of MPCO. V 0121, which is possibly homologous to the neurovascular and dorsal canals of *L. inextricabilis* (Wang *et al.* 2017). This connection is apparently lost in *L. inextricabilis* stage IV and most likely related to the resorption of teeth, so that MPCO. V 0121 seems to best fit a previous stage (plausibly III) of *L. inextricabilis* ontogeny.

#### Ancestral diet & dietary shifts

A carnivorous diet was recovered as ancestral for theropods and kept in most lineages, but with at least two changes to non-carnivorous diets (Fig. 4). One is seen among Maniraptoriformes, with a reversion to carnivory in Paraves, as previously established by Zanno & Makovicky (2011). The other transition occurred among noasaurids, but it is unclear if this happened once at the ancestor of the clade, with a reversion to carnivory in *Masiakasaurus knopfleri*, which we recovered here as the most likely scenario, or if a non-carnivorous diet was independently acquired by *Be. leopoldinae* and *L. inextricabilis*. This ambiguity is not necessarily related to the restricted sampling of noasaurids in our analysis. In fact, even if all putative members of the group are taken into consideration, uncertainties regarding the phylogenetic position of (de Souza *et al.* 2021; Pol *et al.* 2024) and association of jaw elements (Langer *et al.* 2019; Hendrickx *et al.* 2024) to many noasaurids hamper establishing whether the toothlessness of those two taxa are convergent, symplesiomorphic, or even synapomorphic (although this is less likely given their proposed affinities). Finally, the dietary transitions identified in our analyses are more likely to be associated with equal rates of evolution, but unequal rates cannot be discarded (Table S1).

#### Generalized Procrustes & principal components analysis

The GPA shows that two thirds of the variation found in the maxilla dataset is explained by the first three PCs (32.92%, 20.95% and 12.89%; Table S2). PC1 is strongly influenced by the height of the bone and the length of its rostral region, with species showing more negative values

presenting a longer and thinner maxilla, in addition to an antorbital fossa following the same pattern, and species in more positive regions of PC1 having a high, short maxilla and an antorbital fossa that is rostrocaudally narrow and vertically elongated, resembling those of some abelisaurids such as *Carnotaurus sastrei* and *Ekrixinatosaurus novasi* (Fig. S1). In turn, PC2 largely describes variations in the position of the maxillary contacts to the lacrimal and jugal, mainly in the dorsoventral and rostrocaudal axes, respectively. PC2 is also associated with variations in the proportion between the area of the antorbital fossa and the total area of the maxilla, in addition to explaining changes in the angle formed between the rostral margin of the maxilla and the jugal and lacrimal contacts. Here, more negative phylomorphospace regions are occupied by species with deeper maxillae and small antorbital fossae. In turn, more positive regions are occupied by taxa with longer and thinner maxillae, with a large antorbital fossa occupying a major part of the lateral surface of the bone and the jugal contact in a much more caudal position in relation to the lacrimal contact (Fig. S1). Finally, PC3 is mostly related with the position of the points of greatest inflection of both the ascending ramus and the ventral edge of the maxilla, along the rostrocaudal axis. Representatives on the most positive regions of the phylomorphospace have stocky maxillae, with the point of greater inflection of the ascending ramus in a much more rostral position.

In relation to the dentary dataset, only the first two PCs explain more than 10% of the variation (55.2% and 16.1%; Table S2). PC1 is largely related to the position and size of the mandibular fenestra, as well as to the height of the dentary and the position of the contacts with the surangular and angular. Species with more positive values of this PC have a thin dentary and a very reduced or absent mandibular fenestra, whereas more negative regions are occupied by species bearing high and bulky dentaries, with a large mandibular fenestra, in which the contact with the angular is more caudoventral. This resembles the dentaries of oviraptorids, such as *Ba. long*, *Ci. osmolkae* and *K. mckennai* (Fig. S2). PC2 better explains the ‘inversion’ in position of the angular and surangular contacts on the rostrocaudal axis of the dentary, with species in the more negative phylomorphospace regions having the surangular contact caudal to that of the angular, the reverse being the case for species in more positive regions (Fig. S2).

The PCA allows a visual interpretation of the GPA results, showing the morphological relations between species (Fig. 5; Figs S3–S6). The maxilla dataset shows a large overlap in their distribution, with most taxa presenting intermediate PC values and different groups occupying the same phylomorphospace regions. Despite that, comparing some pairs of taxonomic groups shows that they clearly occupy different areas; for example, Paraves vs Ceratosauria, Ceratosauria vs Tyrannosauroidae + Megaraptora,

Tyrannosauroidae + Megaraptora vs Oviraptorosauria, Oviraptorosauria vs 'non-Pennaraptora Maniraptoromorpha', and Oviraptorosauria vs Paraves. On the contrary, the dentary dataset shows a substantial separation between the area occupied by oviraptorids and the other analysed theropods in PC1 (Fig. 5; Figs S5, S6). The only clear exception to that pattern is *Be. leopoldinae*, which occupies a position very close to that of oviraptorids, which justifies testing the hypothesis of morphological convergence between these taxa. There is a partial segregation of carnivore and non-carnivore taxa in dentary phylomorphospace, absent in that of the maxilla (Fig. 5; Figs S3–S6).

### Phylogenetic signal & allometry

The analyses of both datasets resulted in statistically significant values in the allometry test, with a p-value of 0.05 for the maxilla and 0.01 for the dentary, indicating that size strongly influences the shape of both bones. Hence, to statistically control for this factor, all subsequent tests were carried out adding the specimen size to the models. In turn, phylogeny also had a nearly significant influence in shaping the maxilla and dentary, which respectively showed median p-values of 0.06 and 0.05.

### Phylogenetic generalized least squares

As both datasets showed some degree of phylogenetic signal, we performed a PGLS analysis as detailed in the methodology section. The results are listed in Table 1.

### Disparity & evolutionary rates

The patterns recognized when comparing disparity among groups include: non-carnivorous taxa have greater disparity than carnivores in both datasets; oviraptorosaurs show the greatest disparity in both datasets, with a pronounced difference to other groups in that of the dentary, but with values close to those of Paraves and 'non-Pennaraptora Maniraptoromorpha' for the maxilla dataset (Fig. 6; Table 2). Statistically significant differences between taxonomic groups are presented in Table 3, whereas evolutionary rates for each taxonomic and diet group are shown in Figure 6 and Table 2, with those that have statistically significant differences from one another listed in Table 3. As seen for disparity, carnivorous theropods show lower rates of morphological evolution than non-carnivores, both for the maxilla and dentary, although these differences are not statistically significant (Fig. 6; Tables 2, 3). Also as observed for disparity, oviraptorosaurs show the highest rates of morphological evolution

**TABLE 1.** Phylogenetic generalized least square (PGLS) p-values for the maxilla and dentary datasets, with diet, taxonomic group, and size as predictors.

Variable	Maxilla	Dentary
Diet	0.30 (0.05–0.63)	<b>0.02 (0–0.10)</b>
Size: Diet	0.07 (0–0.28)	0.07 (0–0.20)
'Non-Averostra Theropoda'	0.90 (0.31–1)	0.34 (0–0.86)
Size: 'non-Averostra Theropoda'	0.07 (0–0.32)	0.25 (0.01–0.63)
Ceratosauria	0.79 (0.44–0.93)	0.70 (0.15–0.92)
Size: Ceratosauria	0.50 (0.01–0.88)	0.09 (0.01–0.37)
'Non-Coelurosauria Tetanurae'	0.62 (0.24–0.89)	0.66 (0.09–0.94)
Size: 'non-Coelurosauria Tetanurae'	0.87 (0.37–1)	0.80 (0.27–0.99)
Tyrannosauroidae + Megaraptora	0.98 (0.81–1)	0.81 (0.46–0.95)
Size: Tyrannosauroidae + Megaraptora	0.22 (0.01–0.55)	<b>0.04 (0–0.29)</b>
'Non-Pennaraptora Maniraptoromorpha'	0.17 (0.04–0.5)	0.94 (0.80–0.98)
Size: 'non-Pennaraptora Maniraptoromorpha'	0.41 (0.05–0.75)	0.51 (0.14–0.85)
Oviraptorosauria	0.17 (0.04–0.50)	0.94 (0.80–0.98)
Size: Oviraptorosauria	0.41 (0.05–0.75)	0.51 (0.14–0.85)
Paraves	0.10 (0–0.27)	0.09 (0–0.23)
Size: Paraves	0.10 (0–0.48)	<b>0.04 (0–0.19)</b>

Significant results indicated in **bold**.

for the dentary, but similarly high rates were found for the maxilla of 'non-Averostra Theropoda' and, to a lesser extent, also to Ceratosauria.

### Morphological convergence

For the maxilla, no tests with the PCs summing up 95% of the variance resulted in statistically significant values, but the contrary was the case when only PC1 and PC2 were used, validating the convergence hypothesis between the maxillary shape of *Q. sinensis* and troodontids (Table 1). For the dentary, both tests resulted in statistical significance for all four metrics, strongly supporting the hypothesis of convergent evolution regarding the morphology of this bone in *Be. leopoldinae* and Oviraptoridae (Tables 1, 4).

## DISCUSSION

### General patterns

The results presented above show that a considerable part of the morphological variation seen in the maxilla and

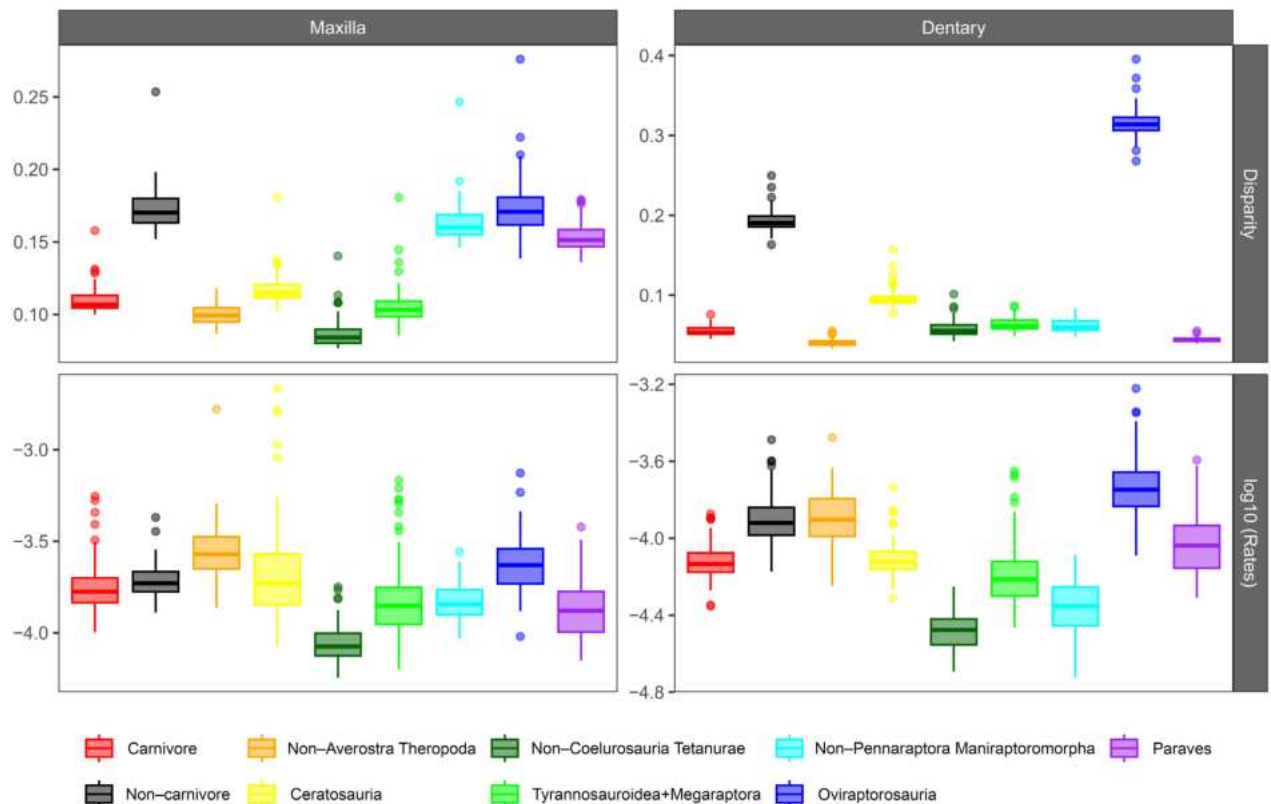


**FIG. 6.** Boxplots depicting the values of disparity and evolutionary rates estimated for dietary and taxonomic groups for the maxilla and dentary. For the evolutionary rates boxplots, values are shown on a  $\log_{10}$  scale.

**TABLE 2.** Disparity and evolutionary rates for the maxilla and dentary datasets, for dietary and taxonomic groups.

Metric	Group	Maxilla	Dentary
Disparity	Carnivores	0.107 (0.101–0.129)	0.053 (0.047–0.067)
	Non-carnivores	0.170 (0.156–0.196)	0.191 (0.173–0.221)
	Ceratosauria	0.115 (0.106–0.135)	0.094 (0.082–0.121)
	Oviraptorosauria	0.171 (0.149–0.210)	0.314 (0.287–0.353)
	Paraves	0.151 (0.140–0.177)	0.044 (0.040–0.051)
	Tyrannosauroidae+Megaraptora	0.103 (0.090–0.133)	0.061 (0.052–0.083)
	'Non-Coelurosauria Tetanurae'	0.084 (0.077–0.108)	0.055 (0.045–0.081)
	'Non-Pennaraptora Maniraptoromorpha'	0.160 (0.148–0.185)	0.060 (0.050–0.079)
	'Non-Averostra Theropoda'	0.099 (0.089–0.115)	0.040 (0.035–0.052)
Rates	Carnivores	0.00017 (0.00012–0.00042)	0.00007 (0.00006–0.00013)
	Non-carnivores	0.00019 (0.00014–0.00028)	0.00012 (0.00008–0.00024)
	Ceratosauria	0.00019 (0.00010–0.00135)	0.00008 (0.00006–0.00013)
	Oviraptorosauria	0.00023 (0.00014–0.00046)	0.00018 (0.00010–0.00043)
	Paraves	0.00013 (0.00008–0.00032)	0.00009 (0.00005–0.00023)
	Tyrannosauroidae+Megaraptora	0.00014 (0.00008–0.00053)	0.00006 (0.00004–0.00019)
	'Non-Coelurosauria Tetanurae'	0.00008 (0.00006–0.00015)	0.00003 (0.00002–0.00005)
	'Non-Pennaraptora Maniraptoromorpha'	0.00014 (0.00010–0.00022)	0.00004 (0.00003–0.00008)
	'Non-Averostra Theropoda'	0.00027 (0.00018–0.00049)	0.00013 (0.00008–0.00022)

dentary of theropods may be explained by the phylogenetic position of the taxa, corroborating the results of Brusatte *et al.* (2012) and Foth & Rauhut (2013) for the

entire skull. In addition, it was also shown that specimen size has a strong influence on modelling the shape of both bones, also corroborating a previous study that

**TABLE 3.** Disparity and evolutionary rates; group comparisons with significant differences for the maxilla and dentary datasets.

Metric	Dataset	Group comparison
Disparity	Maxilla	Carnivores × non-Carnivores
		'Non-Coelurosauria Tetanurae' × Oviraptorosauria
		'Non-Coelurosauria Tetanurae' × Paraves
		'Non-Coelurosauria Tetanurae' × 'non-Pennaraptora Maniraptoromorpha'
	Dentary	Carnivores × non-carnivores
		Ceratosauria × Oviraptorosauria
		Oviraptorosauria × Paraves
		Oviraptorosauria × Tyrannosauroidae+Megaraptora
		'Non-Coelurosauria Tetanurae' × Oviraptorosauria
Rates	Maxilla	'Non-Pennaraptora Maniraptoromorpha' × Oviraptorosauria
		Oviraptorosauria × 'non-Averostra Theropoda'
	Dentary	'Non-Coelurosauria Tetanurae' × Oviraptorosauria
		'Non-Coelurosauria Tetanurae' × 'non-Averostra Theropoda'
		'Non-Pennaraptora Maniraptoromorpha' × Oviraptorosauria

See Table S3 for the complete list of p-values.

found a significant relation between skull shape and size (Brusatte *et al.* 2012). In Dataset 2, a surprising 55.2% of the observed variation in dentary shape is explained by a single principal component, with its phylomorphospace area towards more negative values occupied mainly by oviraptorids. In the disparity analysis, significant values for Dataset 2 were found only for carnivorous vs

non-carnivorous taxa and in the comparisons including oviraptorosaurs. In the evolutionary rates analysis of the same dataset, only three significant rates comparisons were found, two of them involving Oviraptorosauria. Oviraptorosaurs have such an aberrant dentary that its shape is statistically different from those of all other taxonomic groups. Its unique morphology also probably influenced the statistical difference in dentary disparity between carnivorous and non-carnivorous taxa, agreeing with previous studies on the feeding mechanics of theropods (Ma *et al.* 2022).

### *Influence of diet on morphology*

All known plainly carnivorous dinosaurs are theropods (Hendrickx *et al.* 2015), a diet most likely to be ancestral for the group (Ballell *et al.* 2022). This condition underwent several changes throughout the evolutionary history of the clade, with non-avian theropods achieving a wide range of feeding habits such as piscivory, insectivory, omnivory and herbivory (Senter 2005; Zanno & Makovicky 2011; Schade *et al.* 2020), and its living representatives (Aves) bearing one of the most varied diets among all metazoan groups (Miller & Pittman 2021). It has been suggested that dietary shifts toward non-carnivory allowed theropods to explore new, and possibly larger morphospace areas (Zanno *et al.* 2009). This was partially corroborated by Brusatte *et al.* (2012), who noticed that non-carnivorous theropod skulls occupied areas not explored by exclusively carnivorous taxa, although said areas were not larger than those occupied by carnivores. These results are partially supported by the present work.

The dentaries of carnivore and non-carnivore theropods occupy rather different areas of the phylomorphospace: the former group showing minor variations in the horizontal axis and major variations in the vertical axis,

**TABLE 4.** Convergence tests for the maxilla (*Qianzhousaurus sinensis* vs Troodontidae) and dentary (*Berthasaura leopoldinae* vs Oviraptoridae).

PC	Test	Maxilla		Dentary	
		Statistic	p-value	Statistic	p-value
PCs (95%)	Ct1	−0.15 (−0.33 to 0)	0.87 (0.33–0.99)	0.29 (0.05–0.45)	<b>0.01 (0–0.06)</b>
	Ct2	−0.05 (−0.10 to 0)	0.78 (0.31–0.95)	0.10 (0.01–0.21)	<b>0 (0–0.06)</b>
	Ct3	−0.03 (−0.06 to 0)	0.64 (0.29–0.86)	0.06 (0.01–0.12)	<b>0.02 (0–0.09)</b>
	Ct4	−0.01 (−0.01 to 0)	0.61 (0.29–0.81)	0.01 (0–0.03)	<b>0.01 (0–0.07)</b>
PC1-PC2	Ct1	0.87 (0.83 to 0.90)	<b>0 (0–0)</b>	0.57 (0.33–0.70)	<b>0.01 (0–0.07)</b>
	Ct2	0.20 (0.14 to 0.26)	<b>0 (0–0.03)</b>	0.17 (0.06–0.31)	<b>0 (0–0.08)</b>
	Ct3	0.20 (0.13 to 0.26)	<b>0.01 (0–0.07)</b>	0.13 (0.05–0.20)	<b>0.04 (0–0.16)</b>
	Ct4	0.04 (0.03 to 0.05)	<b>0.02 (0–0.06)</b>	0.03 (0.01–0.06)	<b>0 (0–0.08)</b>

Significant results indicated in **bold**.



and the latter showing an inverted trend, as well as a higher disparity in PC1 values. Furthermore, tests comparing the disparity of each dietary group show that carnivores have a statistically significant trend to maintain the height and length of the dentary, whereas non-carnivorous taxa show large variations in these values. Also, PGLS results indicate that diet allows us to clearly separate the dentary shape of theropods, although this is not the case when size is controlled for. This lower variability in carnivores may be the product of functional restrictions associated with predation, as more robust jaws allow for greater biting force, but also lead to a reduction in the speed of closing the mouth. Hence, a carnivorous taxon cannot maximize its bite force without compromising the speed for capturing prey (Ma *et al.* 2022). In turn, lacking this ecological constraint, non-carnivorous theropods explored a greater range of combinations between bite force/speed. For example, oviraptorids specialized in a strong and slow bite (Meade & Ma 2022), and more efficient stress dissipation in the dentary of therizinosaurs allowed a considerably strong bite even with a thinner bone (Lautenschlager 2017).

The maxilla phylomorphospace shows no markedly distinct areas for carnivores and non-carnivores, but the former group occupies a larger area. This variation is more marked in PC2, with carnivores showing both more positive and more negative values. This reveals that carnivores and non-carnivores vary equally in maxillary height and in the length of the rostral region, with the non-carnivorous oviraptorids and the carnivorous abelisaurids occupying similar positive regions of PC1, and some carnivorous (troodontids and spinosaurids) and non-carnivorous (deinocheirids) taxa similar negative regions. At the same time, carnivorous forms show greater variability in relation to the relative size of the antorbital fossa.

Brusatte *et al.* (2012) suggested that the skulls of carnivorous and non-carnivorous theropods have equivalent morphological variability, but concentrated in different areas of the morphospace. Our results for the maxilla tell a different story. Although carnivores occupy a larger area, both dietary groups largely overlap. This indicates that the skull as a whole and the maxilla alone were subjected to different pressures during the evolutionary history of the group. A possible explanation is that anatomical changes associated with bite force, such as muscle attachment areas, are more concentrated in the caudal portion of the skull (Holliday 2009), and have much less effect on elements in the rostral part, such as the maxilla. Indeed, Foth & Rauhut (2013) found that the preorbital module of the theropod skull (which integrates the premaxilla, maxilla, nasal and part of jugal and lacrimal, corresponding well with our dataset) is more influenced by biomechanics than by phylogeny, although with

weaker functional constraint compared to the postorbital region. As for the dentary, the trend found here is very similar to that found by Brusatte *et al.* (2012), with carnivores and non-carnivores occupying subequal-sized areas in very different regions of the phylomorphospace.

### Taxonomic groups

Both datasets show that phylogeny had some influence in shaping of the maxilla and dentary of theropods. Yet, when we analyse each taxonomic group individually, this relationship is not so clear. The PGLS test shows that size-controlled comparisons are statistically significant only for Paraves and Tyrannosauroidae + Megaraptora. This may result from the choice of groups, which are very inclusive and in some cases non-monophyletic. Yet, Oviraptorosauria was the group with more distinctive results in most analyses. They occupy a unique portion of the phylomorphospace of Dataset 2, with highly negative PC1 values for Caenagnathidae and, especially, Oviraptoridae. The only non-oviraptorosaur taxon with similar values is *Be. leopoldinae*, revealing a possible case of evolutionary convergence in the dentary shape. The uniqueness of the oviraptorosaur dentary is further confirmed by the disparity and evolutionary rates tests, which revealed significant differences between the group and all other taxonomic partitions, indicating that the oviraptorosaur dentary is not only distinct from those of other groups, but also highly variable within the clade. Yet, our analysis did not find many differences between the maxilla of oviraptorosaurs and those of other theropods, even though they have the most variable morphology when compared to the other groups. The phylomorphospace graph shows the species of the group relatively concentrated in the positive region of PC1 and negative region of PC2, but not standing out as in the dentary dataset. In fact, they are rather close, sharing most of their area with groups such as Ceratosauria and 'non-Averostra Theropoda'. In addition, although the evolutionary rate tests found no significant differences between oviraptorosaurs and other theropods regarding the shape of the maxilla, the group appears morphologically unique in other studies focused on the entire skull (Brusatte *et al.* 2012; Foth & Rauhut 2013). This may be related to the development of a robust premaxilla in oviraptorosaurs (Meade *et al.* 2024), reducing the need for substantial changes in the maxilla to match those of the lower jaw.

### Morphological convergence

The proximity in phylomorphospace between the maxillae of *Q. sinensis* and troodontids, and the dentaries of

*Be. leopoldinae* and oviraptorids hints at the occurrence of morphological convergence between these taxa. This was confirmed by the convergence test, in which both cases were supported by the PC1&2 analysis, and that of *Be. leopoldinae* and oviraptorids even in the broader analysis of 95% PCs. The latter case came as no surprise, as the compared bones are quite similar in general morphology. In addition to lacking teeth, they are high and bear a large mandibular fenestra, which are features measured by PC1. Yet it is important to note that the occlusal view of the dentary, not tested in our study, reveals a more expanded symphysis in oviraptorids, forming a wider and deeper shelf that could affect jaw functional performance. As for the other convergence case, *Q. sinensis* belongs to Alioramini, a clade of Tyrannosauridae with a divergent long and slender snout (Foster *et al.* 2021) that resembles those of troodontids (Senter *et al.* 2010), as measured by PC1&2 in the form of shallow maxillae with a long rostral portion. Alioramini are hypothesized to have hunted medium-sized terrestrial vertebrates (Foster *et al.* 2021), whereas the feeding habits of troodontids are controversial (Zanno & Makovicky 2011; Freimuth *et al.* 2021; Cullen & Cousens 2024). Indeed, given their discrepant sizes, the convergence in their maxilla shape is likely to be the result of adaptations to different feeding strategies.

*Berthasaura leopoldinae* and most oviraptorids lived in desertic palaeoenvironments (e.g. Jerzykiewicz & Russell 1991; de Souza *et al.* 2021), setting a probable cause for their convergence (i.e. their similar dentaries could be an adaptation to feed on tough xerophytic plants). Yet, despite the prevalence of deserts during the Cretaceous (Chumakov 2004; Hay & Floegel 2012), fossils of plants occupying those landscapes are relatively rare (Vakhrameev 1991; Pires *et al.* 2011). Hence, although a uniformitarian view suggests xeric adaptations as common to plants living in arid areas, regardless of their age, evidence of such adaptations is elusive in the fossil record. Yet, the occurrence of the xeromorphic conifers Cheirolepidiaceae in arid Cretaceous environments has been inferred from *Classopollis* pollen (Vakhrameev 1991; Carvalho *et al.* 2022). This suggests that plants with tough parts were at that time also common in such environments, possibly driving the skeletal convergence of *Be. leopoldinae* and oviraptorids discussed here.

## CONCLUSION

Desertic environments are marginal settings for adaptation of lifeforms, with water restriction, extreme temperatures, and relatively low biomass and primary productivity. Some xerophytic plants respond to these conditions by hardening leaves, stems, fruits and seeds, which in turn serve as food for animals capable of processing such tough vegetative

parts. Yet, this requires special maxillomandibular apparatuses, resistant to abrasion and capable of strong bites. Two well-known arid settings of Cretaceous age include the Early Cretaceous Caiuá palaeodesert, in south-central Brazil (Fernandes *et al.* 2007), and those recorded in several Late Cretaceous deposits of the Gobi Desert (Longrich *et al.* 2010). Indeed, as revealed by the quantitative analyses conducted here, the dinosaur diversity of those faunas includes taxa (i.e. oviraptorids and *Be. leopoldinae*) with a similarly aberrant dentary morphology. This hypothesis passed convergence tests, implying that adaptation to similar environments, separated both geographically and chronologically, by different theropods groups, resulted in the morphological convergence of their main lower jaw bone, including edentulousness. Assuming that such modifications were driven in full or in the most part by diet and that oviraptorids probably feed on hard plant material (Meade & Ma 2022), a similar diet is suggested for *Be. leopoldinae*. Among noasaurids, edentulousness was ontogenetically controlled in *L. inextricabilis*, with adult individuals losing their teeth. This could have also been the case for *Be. leopoldinae*, as revealed by the gross anatomy and  $\mu$ CT data of MPCO. V 0121, which may have died at an ontogenetic stage in which teeth were already lost, but alveolar vestiges can still be recognized in the dentary.

**Acknowledgements.** We thank the funding agencies Fundação de Amparo à Pesquisa do Estado de São Paulo (FAPESP: grants 2023/06692-3 for FFP, 2021/12231-3 for RD, 2022/00044-7 for DMC, and 2020/07997-4 for MCL) and the Conselho Nacional de Desenvolvimento Científico e Tecnológico (CNPq: grant 131092/2024-3 for JAL) for their support of this research. Luke Meade and Michael Pittman commented on an earlier draft of this manuscript.

**Author contributions.** **Conceptualization** Felipe F. Pierossi (FFP), Rafael Delcourt (RD), Daniel de Melo Casali (DMC), Max C. Langer (MCL); **Data Curation** FFP, DMC, Neurides de Oliveira Martins (NOM), Paulo Manzig (PM); **Formal Analysis** FFP, RD, DMC, MCL; **Funding Acquisition** FFP, RD, DMC, NOM, MCL; **Investigation** FFP, RD, DMC, João A. Leme (JAL), MCL; **Methodology** FFP, RD, DMC, MCL; **Project Administration** RD, NOM, MCL; **Resources** FFP, RD, DMC, NOM, PM, MCL; **Supervision** MCL; **Validation** FFP, DMC; **Visualization** FFP, RD, DMC, JAL, MCL; **Writing – Original Draft Preparation** FFP, RD, DMC, JAL, MCL; **Writing – Review & Editing** FFP, RD, DMC, MCL.

## DATA ARCHIVING STATEMENT

Data for this study are available in MorphoSource: <https://doi.org/10.17602/M2/M703609> and the Dryad Digital Repository: <https://doi.org/10.5061/dryad.p5hqbkzkw>

**Editor.** David Button

## SUPPORTING INFORMATION

Additional Supporting Information can be found online (<https://doi.org/10.1111/pala.70014>):

**Appendix S1.** Sources of maxilla and dentary images used in this study.

**Appendix S2.** Landmark descriptions.

**Appendix S3.** The phylogenetic relationships among more inclusive groups of Theropoda.

**Figure S1.** Minimum and maximum shape configurations corresponding to the two first principal components (PC1–PC2) of the maxillaries of sampled theropods.

**Figure S2.** Minimum and maximum shape configurations corresponding to the two first principal components (PC1–PC2) of the dentaries of sampled theropods.

**Figure S3.** Phylomorphospaces depicting the first two principal components (PCs) for the maxilla, coloured by dietary groups, as in Figure 5, but with the indication of all taxon names.

**Figure S4.** Phylomorphospaces depicting the first two principal components (PCs) for the maxilla, coloured by taxonomic groups, as in Figure 5, but with the indication of all taxon names.

**Figure S5.** Phylomorphospaces depicting the first two principal components (PCs) for the dentary, coloured by dietary groups, as in Figure 5, but with the indication of all taxon names.

**Figure S6.** Phylomorphospaces depicting the first two principal components (PCs) for the dentary, coloured by taxonomic groups, as in Figure 5, but with the indication of all taxon names.

**Table S1.** Summary of model fitting of equal (ER) and unequal rates (ARD) models of discrete character evolution, applied to the dietary categories for conducting ancestral state estimations.

**Table S2.** Summary of principal component (PC) analyses results for maxilla and dentary datasets.

**Table S3.** Summary of p-values for disparity and evolutionary rates' group comparisons for maxilla and dentary datasets.

## REFERENCES

- Adams, D. C. 2014a. A generalized *K* statistic for estimating phylogenetic signal from shape and other high-dimensional multivariate data. *Systematic Biology*, **63**, 685–697.
- Adams, D. C. 2014b. A method for assessing phylogenetic least squares models for shape and other high-dimensional multivariate data. *Evolution*, **68**, 2675–2688.
- Adams, D. C. 2014c. Quantifying and comparing phylogenetic evolutionary rates for shape and other high-dimensional phenotypic data. *Systematic Biology*, **63**, 166–177.
- Adams, D., Collyer, M., Kaliontzopoulou, A. and Baken, E. 2024. geomorph: software for geometric morphometric analyses. R package version 4.0.7. <https://cran.r-project.org/package=geomorph>
- Allain, R. 2002. Discovery of megalosaur (Dinosauria, Theropoda) in the middle Bathonian of Normandy (France) and its implications for the phylogeny of basal Tetanurae. *Journal of Vertebrate Paleontology*, **22**, 548–563.
- Aranciaga Rolando, A. M., Motta, M. J., Agnolín, F. L., Manabe, M., Tsuihiji, T. and Novas, F. E. 2022. A large Megaraptoridae (Theropoda: Coelurosauria) from Upper Cretaceous (Maastrichtian) of Patagonia, Argentina. *Scientific Reports*, **12**, 6318.
- Ballell, A., Benton, M. J. and Rayfield, E. J. 2022. Dental form and function in the early feeding diversification of dinosaurs. *Science Advances*, **8**, abq5201.
- Bapst, D. W. 2012. paleotree: an R package for paleontological and phylogenetic analyses of evolution. *Methods in Ecology and Evolution*, **3**, 803–807.
- Barr, W. A. 2017. ggphylomorpho, version 0.2. <https://github.com/wabarr/ggphylomorpho>
- Barrett, P. M. 2005. The diet of ostrich dinosaurs (Theropoda: Ornithomimosauria). *Palaeontology*, **48**, 347–358.
- Blomberg, S. P., Garland, T. and Ives, A. R. 2003. Testing for phylogenetic signal in comparative data: behavioral traits are more labile. *Evolution*, **57**, 717–745.
- Brusatte, S. L. and Carr, T. D. 2016. The phylogeny and evolutionary history of tyrannosaurid dinosaurs. *Scientific Reports*, **6**, 20252.
- Brusatte, S. L. and Sereno, P. C. 2008. Phylogeny of Allosauroidae (Dinosauria: Theropoda): comparative analysis and resolution. *Journal of Systematic Palaeontology*, **6**, 155–182.
- Brusatte, S. L., Sakamoto, M., Montanari, S. and Herculano Smith, W. E. H. 2012. The evolution of cranial form and function in theropod dinosaurs: insights from geometric morphometrics. *Journal of Evolutionary Biology*, **25**, 365–377.
- Canale, J. I., Apesteguía, S., Gallina, P. A., Mitchell, J., Smith, N. D., Cullen, T. M., Shinya, A., Haluza, A., Gianechini, F. A. and Makovicky, P. J. 2022. New giant carnivorous dinosaur reveals convergent evolutionary trends in theropod arm reduction. *Current Biology*, **32**, 3195–3202.e5.
- Carrano, M. T., Sampson, S. D. and Forster, C. A. 2002. The osteology of *Masiakasaurus knopfleri*, a small abelisauroid (Dinosauria: Theropoda) From the Late Cretaceous of Madagascar. *Journal of Vertebrate Paleontology*, **22**, 510–534.
- Carrano, M. T., Benson, R. B. J. and Sampson, S. D. 2012. The phylogeny of Tetanurae (Dinosauria: Theropoda). *Journal of Systematic Palaeontology*, **10**, 211–300.
- Carvalho, M. A., Lana, C. C., Sá, N. P., Santiago, G., Giannnerini, M. C. S. and Bengtson, P. 2022. Influence of the intertropical convergence zone on early cretaceous plant distribution in the South Atlantic. *Scientific Reports*, **12**, 12600.
- Cau, A. 2024. A unified framework for predatory dinosaur macroevolution. *Bollettino della Società Paleontologica Italiana*, **63**, 1–19.
- Chumakov, M. N. 2004. Trends in global climate changes inferred from geological data. *Stratigraphy and Geological Correlation*, **12**, 117–138.
- Collyer, M. and Adams, D. 2024. RRPP: Linear Model Evaluation with Randomized Residuals in a Permutation Procedure. R package version 2.0.0. <https://cran.r-project.org/package=RRPP>
- Cuesta, E., Vidal, D., Ortega, F., Shibata, M. and Sanz, J. L. 2022. *Pelecanimimus* (Theropoda: Ornithomimosauria) postcranial anatomy and the evolution of the specialized manus in Ornithomimosauria and sternum in maniraptoriforms. *Zoological Journal of the Linnean Society*, **194**, 553–591.

- Cullen, T. M. and Cousens, B. L. 2024. New biogeochemical insights into Mesozoic terrestrial paleoecology and evidence for omnivory in troodontid dinosaurs. *Bulletin of the Geological Society of America*, **136**, 2689–2701.
- Ernesto, M., Batezelli, A., Saad, A. R., Caminha-Maciel, G. and Oliveira, P. G. 2024. Post-magmatic sedimentation in the Paraná Basin, Brazil: paleomagnetic constraints on the age of the Cretaceous Caiuá Group. *Boletín de la Sociedad Geológica Mexicana*, **76**, A160124.
- Felsenstein, J. 1985. Phylogenies and the comparative method. *American Naturalist*, **125**, 1–15.
- Fernandes, L., Decastro, A. and Basilici, G. 2007. Seismites in continental sand sea deposits of the Late Cretaceous Caiuá Desert, Bauru Basin, Brazil. *Sedimentary Geology*, **199**, 51–64.
- Foster, W., Brusatte, S. L., Carr, T. D., Williamson, T. E., Yi, L. and Lü, J. 2021. The cranial anatomy of the long-snouted tyrannosaurid dinosaur *Qianzhousaurus sinensis* from the Upper Cretaceous of China. *Journal of Vertebrate Paleontology*, **41**, e1999251.
- Foth, C. and Rahut, O. W. M. 2013. Macroevolutionary and morphofunctional patterns in theropod skulls: a morphometric approach. *Acta Palaeontologica Polonica*, **58**, 1–16.
- Freimuth, W. J., Varricchio, D. J., Brannick, A. L., Weaver, L. N. and Wilson Mantilla, G. P. 2021. Mammal-bearing gastric pellets potentially attributable to *Troodon formosus* at the Cretaceous Egg Mountain locality, Two Medicine Formation, Montana, USA. *Palaeontology*, **64**, 699–725.
- Grossnickle, D. M., Brightly, W. H., Weaver, L. N., Stanchak, K. E., Roston, R. A., Pevsner, S. K., Stayton, C. T., Polly, P. D. and Law, C. J. 2024. Challenges and advances in measuring phenotypic convergence. *Evolution*, **78**, 1355–1371.
- Hasegawa, H., Tada, R., Ichinnorov, N. and Minjin, C. 2009. Lithostratigraphy and depositional environments of the Upper Cretaceous Djadokhta Formation, Ulan Nuur basin, southern Mongolia, and its paleoclimatic implication. *Journal of Asian Earth Sciences*, **35**, 13–26.
- Hay, W. W. and Floegel, S. 2012. New thoughts about the Cretaceous climate and oceans. *Earth-Science Reviews*, **115**, 262–272.
- Hendrickx, C., Hartman, S. A. and Mateus, O. 2015. An overview of non-avian theropod discoveries and classification. *PalArch's Journal of Vertebrate Palaeontology*, **12** (1), 1–73.
- Hendrickx, C., Cerroni, M. A., Agnolín, F. L., Catalano, S., Ribeiro, C. F. and Delcourt, R. 2024. Osteology, relationship, and feeding ecology of the theropod dinosaur *Noasaurus leali* from the Late Cretaceous of North-Western Argentina. *Zoological Journal of the Linnean Society*, **202**, zlae150.
- Holliday, C. M. 2009. New insights into dinosaur jaw muscle anatomy. *The Anatomical Record*, **292**, 1246–1265.
- Jasinski, S. E., Sullivan, R. M. and Dodson, P. 2020. New dromaeosaurid dinosaur (Theropoda, Dromaeosauridae) from New Mexico and biodiversity of dromaeosaurids at the end of the Cretaceous. *Scientific Reports*, **10**, 5105.
- Jerzykiewicz, T. and Russell, D. A. 1991. Late Mesozoic stratigraphy and vertebrates of the Gobi Basin. *Cretaceous Research*, **12**, 345–377.
- Ji, Q., Currie, P. J., Norrell, M. A. and Ji, S. A. 1998. Two feathered dinosaurs from northeastern China. *Nature*, **393**, 753–761.
- Kassambara, A. 2023. rstatix: pipe-friendly framework for basic statistical tests. R package version 0.7.2. <https://cran.r-project.org/package=rstatix>
- Kellner, A. W. A., Weinschütz, L. C., Holgado, B., Bantim, R. A. M. and Sayão, J. M. 2019. A new toothless pterosaur (Pterodactyloidea) from southern Brazil with insights into the paleoecology of a Cretaceous desert. *Anais da Academia Brasileira de Ciências*, **91** (suppl. 2), e20190768.
- Langer, M. C., de Oliveira Martins, N., Manzig, P. C., de Souza Ferreira, G., De Almeida Marsola, J. C., Fortes, E., Lima, R., Sant'ana, L. C. F., Da Silva Vidal, L., Da Silva Lorençato, R. H. and Ezcurra, M. D. 2019. A new desert-dwelling dinosaur (Theropoda, Noasaurinae) from the Cretaceous of south Brazil. *Scientific Reports*, **9**, 1–31.
- Lautenschlager, S. 2017. Functional niche partitioning in Therizinosauria provides new insights into the evolution of theropod herbivory. *Palaeontology*, **60**, 375–387.
- Lewis, P. O. 2001. A likelihood approach to estimating phylogeny from discrete morphological character data. *Systematic Biology*, **50**, 913–925.
- Longrich, N. and Currie, P. 2009. *Albertonykus borealis*, a new alvarezsaur (Dinosauria: Theropoda) from the Early Maastriichtian of Alberta, Canada: implications for the systematics and ecology of the Alvarezsauridae. *Cretaceous Research*, **30**, 239–252.
- Longrich, N. R., Currie, P. J. and Zhi-Ming, D. 2010. A new oviraptorid (Dinosauria: Theropoda) from the Upper Cretaceous of Bayan Mandahu, Inner Mongolia. *Palaeontology*, **53**, 945–960.
- Lü, J., Pu, H., Kobayashi, Y., Xu, L., Chang, H., Shang, Y., Liu, D., Lee, Y. N., Kundrát, M. and Shen, C. 2015. A new oviraptorid dinosaur (Dinosauria: Oviraptorosauria) from the Late Cretaceous of southern China and its paleobiogeographical implications. *Scientific Reports*, **5**, 11490.
- Ma, W., Pittman, M., Butler, R. J. and Lautenschlager, S. 2022. Macroevolutionary trends in theropod dinosaur feeding mechanics. *Current Biology*, **32**, 677–686.e3.
- Maddison, W. P. and Maddison, D. R. 2023. Mesquite: a modular system for evolutionary analysis. Version 3.81. <http://www.mesquiteproject.org>
- Manzig, P. C., Kellner, A. W. A., Weinschütz, L. C., Frago, C. E., Vega, C. S., Guimarães, G. B., Godoy, L. C., Liccardo, A., Ricetti, J. H. Z. and De Moura, C. C. 2014. Discovery of a rare pterosaur bone bed in a Cretaceous desert with insights on ontogeny and behavior of flying reptiles. *PLoS One*, **9**, e100005.
- Marsh, A. D. and Rowe, T. B. 2020. A comprehensive anatomical and phylogenetic evaluation of *Dilophosaurus wetherilli* (Dinosauria, Theropoda) with descriptions of new specimens from the Kayenta Formation of northern Arizona. *Journal of Paleontology*, **94** (S78), 1–103.
- Marugán-Lobón, J. and Buscalioni, Á. D. 2004. Geometric morphometrics in macroevolution: morphological diversity of the skull in modern avian forms in contrast to some theropod dinosaurs. 157–173. In Elewa, A. M. T. (ed.) *Morphometrics*. Springer.
- Meade, L. E. and Ma, W. 2022. Cranial muscle reconstructions quantify adaptation for high bite forces in Oviraptorosauria. *Scientific Reports*, **12**, 3010.



- Meade, L. E., Pittman, M., Balanoff, A. and Lautenschlager, S. 2024. Cranial functional specialisation for strength precedes morphological evolution in Oviraptorosauria. *Communications Biology*, **7**, 436.
- Miller, C. V. and Pittman, M. 2021. The diet of early birds based on modern and fossil evidence and a new framework for its reconstruction. *Biological Reviews*, **96**, 2058–2112.
- Nesbitt, S. J., Smith, N. D., Irmis, R. B., Turner, A. H., Downs, A. and Norell, M. a. 2009. A complete skeleton of a Late Triassic saurischian and the early evolution of dinosaurs. *Science*, **326**, 1530–1533.
- O'Higgins, P. 2000. The study of morphological variation in the hominid fossil record: biology, landmarks and geometry. *Journal of Anatomy*, **197**, 103–120.
- Pagel, M. 1994. Detecting correlated evolution on phylogenies: a general method for the comparative analysis of discrete characters. *Proceedings of the Royal Society B*, **255** (1342), 6.
- Paradis, E., Claude, J. and Strimmer, K. 2004. APE: Analyses of phylogenetics and evolution in R language. *Bioinformatics*, **20**, 289–290.
- Pêgas, R. 2025. A taxonomic note on the tapejarid pterosaurs from the Pterosaur Graveyard Site (Caiuá Group, ?Early Cretaceous of Southern Brazil): evidence for the presence of two species. *Historical Biology*, **37**, 1277–1298.
- Pierossi, F. F., Delcourt, R., Casali, D. M., Leme, J. A., Martins, N. O., Manzig, P. and Langer, M. C. 2025a. Data from: convergent evolution among non-carnivorous, desert-dwelling theropods as revealed by the dentary of the noasaurid *Berthasaura leopoldinae* (Cretaceous of Brazil) [dataset]. MorphoSource. <https://doi.org/10.17602/M2/M703609>
- Pierossi, F. F., Delcourt, R., Casali, D. M., Leme, J. A., Martins, N. O., Manzig, P. and Langer, M. C. 2025b. Data from: Convergent evolution among non-carnivorous, desert-dwelling theropods as revealed by the dentary of the noasaurid *Berthasaura leopoldinae* (Cretaceous of Brazil) [dataset]. Dryad Digital Repository. <https://doi.org/10.5061/dryad.p5hqbzkzw>
- Pires, E. F., Guerra-Sommer, M., Scherer, C. M., Dos, S., Santos, A. R. and Cardoso, E. 2011. Early Cretaceous coniferous woods from a paleoerg (Paraná Basin, Brazil). *Journal of South American Earth Sciences*, **32**, 96–109.
- Pol, D., Baiano, M. A., Černý, D., Novas, F. E., Cerda, I. A. and Pittman, M. 2024. A new abelisaurid dinosaur from the end Cretaceous of Patagonia and evolutionary rates among the Ceratosauria. *Cladistics*, **40**, 307–356.
- R Core Team. 2024. R: A language and environment for statistical computing. R Foundation for Statistical Computing, Vienna, Austria. <https://www.R-project.org/>
- Revell, L. J. 2024. phytools: phylogenetic tools for comparative biology (and other things). R package version 1.8.5. <https://cran.r-project.org/package=phytools>
- Rohlf, F. J. 2010. tpsDig v2.16. <https://www.sbmorphometrics.org/soft-dataacq.html>
- Ronquist, F., Teslenko, M., Van Der Mark, P., Ayres, D. L., Darling, A., Höhna, S., Larget, B., Liu, L., Suchard, M. A. and Huelsenbeck, J. P. 2012. MrBayes 3.2: efficient Bayesian phylogenetic inference and model choice across a large model space. *Systematic Biology*, **61**, 539–542.
- Sales, M. A. F., Cascon, P. and Schultz, C. L. 2014. Note on the paleobiogeography of Compsognathidae (Dinosauria: Theropoda) and its paleoecological implications. *Anais da Academia Brasileira de Ciências*, **86**, 127–134.
- Sampson, S. D. and Witmer, L. M. 2007. Craniofacial anatomy of *Majungasaurus crenatissimus* (Theropoda: Abelisauridae) from the Late Cretaceous of Madagascar. *Journal of Vertebrate Paleontology*, **27**, 32–102.
- Schade, M., Rauhut, O. W. M. and Evers, S. W. 2020. Neuroanatomy of the spinosaurid *Irritator challengerii* (Dinosauria: Theropoda) indicates potential adaptations for piscivory. *Scientific Reports*, **10**, 9259.
- Schauberger, P. and Walker, A. 2023. openxlsx: read, write and edit xlsx files. R package version 4.2.5.2. <https://CRAN.R-project.org/package=openxlsx>
- Senter, P. 2005. Function in the stunted forelimbs of *Mononykus olecranus* (Theropoda), a dinosaurian anteater. *Paleobiology*, **31**, 373–381.
- Senter, P., Kirkland, J. I., Bird, J. and Bartlett, J. A. 2010. A new troodontid theropod dinosaur from the Lower Cretaceous of Utah. *PLoS One*, **5**, 14329.
- Sereno, P. C. and Novas, F. E. 1994. The skull and neck of the basal theropod *Herrerasaurus ischigualastensis*. *Journal of Vertebrate Paleontology*, **13**, 451–476.
- Simões, T. R., Wilner, E., Caldwell, M. W., Weinschütz, L. C. and Kellner, A. W. A. 2015. A stem acrodontan lizard in the Cretaceous of Brazil revises early lizard evolution in Gondwana. *Nature Communications*, **6**, 8149.
- Smith, D. 1992. The type specimen of *Oviraptor philoceratops*, a theropod dinosaur from the Upper Cretaceous of Mongolia. *Neues Jahrbuch für Geologie und Paläontologie, Abhandlungen*, **186**, 365–388.
- de Souza, G. A., Soares, M. B., Weinschütz, L. C., Wilner, E., Lopes, R. T., De Araújo, O. M. O. and Kellner, A. W. A. 2021. The first edentulous ceratosaur from South America. *Scientific Reports*, **11**, 22281.
- Stayton, C. T. 2015. The definition, recognition, and interpretation of convergent evolution, and two new measures for quantifying and assessing the significance of convergence. *Evolution*, **69**, 2140–2153.
- Sues, H.-D., Nesbitt, S. J., Berman, D. S. and Henrici, A. C. 2011. A late-surviving basal theropod dinosaur from the latest Triassic of North America. *Proceedings of the Royal Society B*, **278**, 3459–3464.
- Symonds, M. R. E. and Blomberg, S. P. 2014. A primer on phylogenetic generalised least squares. 105–130. In Garamszegi, L. Z. (ed.) *Modern phylogenetic comparative methods and their application in evolutionary biology: Concepts and practice*. Springer.
- Tsuihiji, T., Watabe, M., Tsogtbaatar, K. and Barsbold, R. 2016. Dentaries of a caenagnathid (Dinosauria: Theropoda) from the Nemegt Formation of the Gobi Desert in Mongolia. *Cretaceous Research*, **63**, 148–153.
- Vakhrameev, V. A. 1991. *Jurassic and Cretaceous floras and climates of the Earth*. Cambridge University Press.
- Wang, S., Stigler, J., Amiot, R., Wang, X., Du, G.-H., Clark, J. M. and Xu, X. 2017. Extreme ontogenetic changes in a Ceratosaurian Theropod. *Current Biology*, **27**, 144–148.

- Wickham, H. 2016. *ggplot2: Elegant graphics for data analysis*. Springer. <https://ggplot2.tidyverse.org>
- Xing, L., Miyashita, T., Wang, D., Niu, K. and Currie, P. J. 2020. A new compsognathid theropod dinosaur from the oldest assemblage of the Jehol Biota in the Lower Cretaceous Huajiyang Formation, northeastern China. *Cretaceous Research*, **107**, 104285.
- Xu, X., Cheng, Y. N., Wang, X. L. and Chang, C. H. 2002. An unusual oviraptorosaurian dinosaur from China. *Nature*, **419**, 291–293.
- Xu, X., Zheng, X. and You, H. 2009. A new feather type in a nonavian theropod and the early evolution of feathers. *Proceedings of the National Academy of Sciences*, **106**, 832–834.
- You, H. L., Azuma, Y., Wang, T., Wang, Y. M. and Dong, Z. M. 2014. The first well-preserved coelophysoid theropod dinosaur from Asia. *Zootaxa*, **3873**, 233–249.
- Zaher, H., Pol, D., Navarro, B. A., Delcourt, R. and Carvalho, A. B. 2020. An Early Cretaceous theropod dinosaur from Brazil sheds light on the cranial evolution of the Abelisauridae. *Comptes Rendus Palevol*, **19**, 101.
- Zanno, L. E. and Makovicky, P. J. 2011. Herbivorous ecomorphology and specialization patterns in theropod dinosaur evolution. *Proceedings of the National Academy of Sciences*, **108**, 232–237.
- Zanno, L. E., Gillette, D. D., Albright, L. B. and Titus, A. L. 2009. A new North American therizinosaurid and the role of herbivory in 'predatory' dinosaur evolution. *Proceedings of the Royal Society B*, **276**, 3505–3511.
- Zelditch, M. L., Swiderski, D. L. and Sheets, H. D. 2012. *Geometric morphometrics for biologists: A primer*, Second edition. Academic Press.
- Zhang, C., Stadler, T., Klopstein, S., Heath, T. A. and Ronquist, F. 2016. Total-evidence dating under the fossilized birth–death process. *Systematic Biology*, **65**, 228–249.